The Gap between Experiment and Simulation: Grid Forming Inverter Control during Islanding Transition

Kai Baumgarten, Jan Wachter, Friedrich Wiegel, Richard Jumar, Veit Hagenmeyer
Institute for Automation and Applied Informatics
Karlsruhe Institute of Technology
Eggenstein-Leopoldshafen, Germany
kai.baumgarten@kit.edu

***Abstract*—In order to integrate distributed energy resources into the power grid, grid forming inverters have gained popularity in research activities over the past two decades. Simulated models have long been used to analyze developed control strategies, but their real-world applicability often remains untested. The present article aims to spotlight this gap between simulation and real implementation of the same inverter control scheme. For this, the transition of a stand-alone system from grid-connected to island mode is exemplarily investigated. Good agreement of the dynamics of time-averaged quantities is observed, but the simulation shows limited representation of fast timescale effects. Furthermore, hidden challenges related to the implementation and operation of the experiment are addressed.**

***Index Terms*—grid-forming inverter, microgrid, islanding, experimental validation, droop control, virtual impedance**

I. Introduction

In the evolving landscape of electrical power systems, the increasing penetration of distributed energy resources (DER) such as wind and photovoltaic ones is a main driver of research in the field of power electronic converters. With increasing share of generation, the use of conventional grid-following (GFL) inverters can lead to stability problems [1], [2]. In contrast, grid-forming (GFM) inverters are advantageous in weak grid situations (i.e. low grid short circuit ratio (SCR) due to high share of inverters) [1]. Therefore, the concept of GFM inverter has been gaining popularity in the research community over the last two decades, as demonstrated by the amount of proposed control algorithms, see e.g. [3]–[6].

For the development and analysis of control strategies for inverters, time domain simulations are an essential and widely applied tool [7]. However, the degree of agreement between the behavior of the simulation model and the physical system highly depends on the chosen modelling approach and detail. In particular, significant deviations can occur in the case of transient events such as the disconnection of a microgrid.

Control strategies focusing on the transition between operation modes of grid forming inverters are proposed in [7], [8], but only validated via simulations. The authors of [9] propose a a seamless transition method and present experiments of the re-connection to the grid. In [10], a controller for seamless transition to islanding is proposed in a case with three inverters including experimental validation. The authors of [11] experimentally verify a proposed strategy for seamless transition between operation modes.

Further publications in the field of grid forming inverters which include both simulation and experiments are [12]–[18]. While [12], [13] consider scenarios with parallel inverters, [14] focus on interaction with a wind turbine. The authors of [15] analyze a stand-alone inverter but do not investigate on the transition between operation modes. For [16], [17], a direct comparability of simulation and experimental results is not given. In this sense, [18] deserves special consideration because the authors achieve clear comparability by presenting simulation and experimental results in the same graphs. The considered system consists of an inverter parallel to a synchronous generator, to which load steps are applied.

To the best of the authors present knowledge, no in-depth comparison between experiment and simulation has been performed focusing on the transition between grid-connected and islanding mode of a stand-alone inverter system. The present paper introduces precisely such comparison using the same control code in both simulation and experiment to address the respective gap.

The remainder of the article is structured as follows: Section II presents the considered test case. Section III defines the methodology including experimental setup and simulation. The results are presented and discussed in Section IV. Implementation challenges are described in Section V, while section VI summarizes the findings.

II. Case Study

For a stand-alone grid forming inverter, the transition from the operation mode grid-connected to islanding is investigated.

A. Testing Objective

The testing objective is as follows: A) Examine the temporal behavior of transient after disconnection from grid for both simulation and experiment. B) Compare steady state before and after disconnection for simulation and experiment.

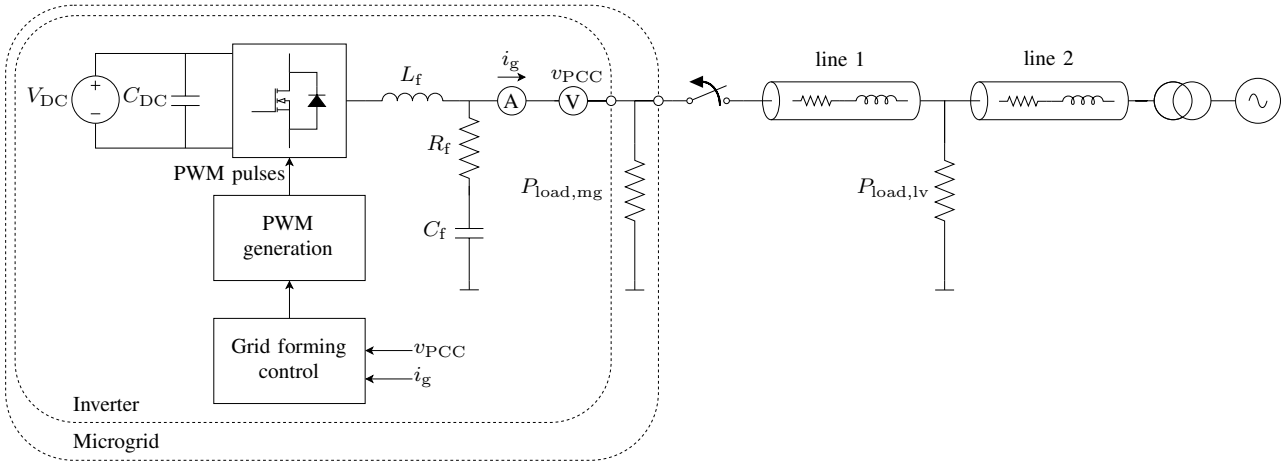

Fig. 1. Single line diagram of the analyzed system.

B. Performance Metrics

The considered quantities are voltage and current (RMS and waveform), active and reactive power and frequency. The performance metrics are: A) dynamic behavior of quantities during transient, i.e. trend, number of peaks, settling time. B) steady state deviation of quantities, total harmonic distortion (THD) of voltage and current.

C. Test Scenario

The islanding test case represents the scenario of a microgrid disconnecting from the public grid as the frequency of the grid is at its operational limit of 50.5 Hz [19]. At $t = 0\,\mathrm{s}$, the microgrid is disconnected from the public grid. During the whole scenario, the reference values $P_{\mathrm{ref}} = 3\,\mathrm{kW}$ and $Q_{\mathrm{ref}} = 0\,\mathrm{kvar}$ of the droop control of the inverter are kept constant.

D. System Topology

The system under test is shown in Fig. 1. It consists out of a microgrid connected to a low voltage network. The microgrid includes a grid-forming inverter of $P_{\mathrm{nom,inv}} = 10\,\mathrm{kW}$ rated power and a resistance load of $P_{\mathrm{load,mg}} = 2\,\mathrm{kW}$. It is placed at the end of a long line, behind the main load of the network of $P_{\mathrm{load,lv}} = 26\,\mathrm{kW}$. The low voltage lines have a R/X ratio of 5.77.

The parameters of the two-level inverter with LC-filter, cf. Fig. 1, are listed in Table I. Fig. 2 depicts the deployed control structure and the control parameters are summarized in Table I. It is a cascaded dq-control with inner current and outer voltage loop. The voltage reference and current phase angle are determined by $P-f$ and $Q-V$ droop. Both droop factors are referred to the nominal power of the inverter. The decoupling of $P-f$ and $Q-V$ is only valid in the case of an inductive grid, which is not given in the low voltage network. Therefore, a virtual impedance is implemented in order to ensure stable operation of the droop control in the case of a resistive grid [20].

TABLE I
GRID FORMING INVERTER PARAMETERS.

Description	Parameter	Value
Nominal power	P_{nom}	10 kW
Nominal voltage	V_{nom}	400 V
Nominal frequency	f_0	50 Hz
Switching frequency	f_{s}	20 kHz
DC link voltage	V_{DC}	750 V
DC link capacitor	$C_{\mathrm{DC,exp1}}$	705 μF
	$C_{\mathrm{DC,exp2}}$	1500 μF
Grid filter	L_{f}, C_{f}, R_{f}	2.36 mH, 10 μF, 1 Ω
EMC filter	L_1, R_1	0.95 mH, 680 kΩ
	C_1, C_2	2.2 μF, 220 nF
Control parameters		
Voltage loop control	k_{pv}, k_{iv}	0.044, 0.8
Current loop control	k_{pi}, k_{ii}	0.833, 83
P-f droop factor	m	25.46 %
Q-V droop factor	n	4.77 %
Virtual impedance	R_{vi}, L_{vi}	0.5 Ω, 10 mH
PLL control	$k_{\mathrm{p,PLL}}$, $k_{\mathrm{i,PLL}}$	5, 2

III. METHODOLOGY

A. Experimental Setup

The low voltage network is provided using the laboratory infrastructure presented in [21]. The microgrid is formed by adding an adjustable resistance load directly connected to the inverter. All connections on the low-voltage side of the transformer are realized via five-wire cables, thus including the neutral conductor and protective earth (PE). The loads are star-connected to neutral. For the inverter, the imperix[1] rapid control prototyping solution is used. The control structure of the inverter is designed in MATLAB Simulink and compiled to run on the internal controller. Furthermore, two experiment systems are used, which have slightly different half-bridge modules: PEB8024 (denoted by exp1) and PEB8038 (denoted by exp2). In particular, the current ratings of the semiconductors and the capacity of the DC-link capacitors vary. The inverter setup is connected as displayed in Fig. 3.

[1] https://imperix.com/

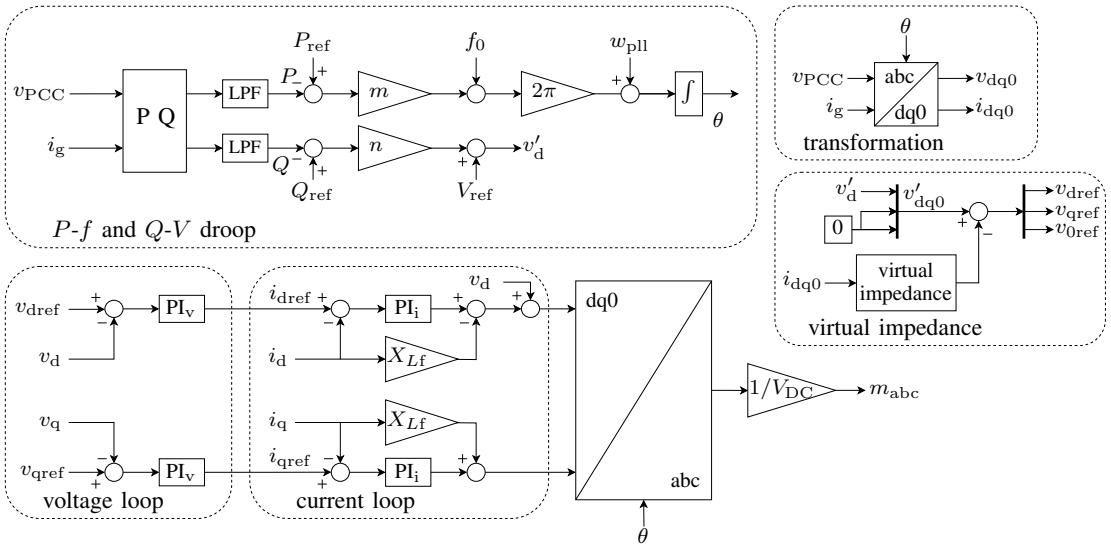

Fig. 2. Control structure of grid forming inverter.

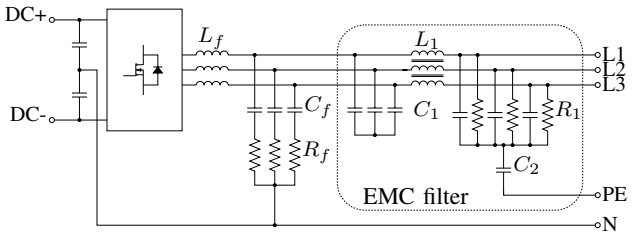

Fig. 3. Three phase topology of inverter setup in experiment including EMC filter.

The neutral conductor is included to account for asymmetry. An electromagnetic compatibility (EMC) filter is included to account for common mode and differential mode interferences, which are due to parasitic coupling. The filter capacitors and inductors can be neglected at relevant grid frequencies and are therefore not considered in simulation.

B. Simulation

The simulation is performed with MATLAB Simulink. The control system is simulated with a fixed step size of $t_{\text{step,c}} = 50\,\mu\text{s}$. A sample and hold delay of $0.1\,t_{\text{step,c}}$ is included accounting for tasks such as data acquisition, read and write processes. In the physical system, symmetry is generally assumed and no neutral conductor is included in the simulation. The time step of the physical system is chosen to be $t_{\text{step,p}} = 200\,\text{ns}$ in order to ensure a sufficient resolution of the duty cycle.

C. Calculation of Time-Averaged Quantities

In the following, the calculation of quantities depicted in Fig. 4 is described. All quantities are derived from 20 kHz raw data of voltages and currents. Due to the varying frequency in the test case, the calculation of RMS values is not straight forward. For example, using a fixed window size of 200 ms can lead to oscillations at frequencies $f \neq 50\,\text{Hz}$. Therefore, the RMS values of voltages are calculated for each interval between two positive zero crossings. Thus, the window size is continuously adapted. This method can not be used for the currents without further adjustments, as multiple positive zero crossings may occur within one fundamental frequency period. Therefore, the current RMS value is calculated with a fixed window size of 19.5 ms, which is suited for the steady state frequency in islanding mode, as this is the most relevant part. For the three phase active and reactive power, the same window size is used for calculating the mean value. It yields sufficient results in slightly asymmetric cases.

IV. Results and Discussion

In Fig. 4, the results of the islanding transition are shown. After disconnection, all quantities settle to a steady state after about 2 s. The trend of the transient as well as the number of peaks and the settling time is similar between both experiments and simulation for all quantities. The time to steady state is about 2 s. During the whole transition, the voltage is within the tolerance band of $\pm 10\,\%$ [19]. Before disconnection, the steady state voltage is low due to the voltage drop along the low voltage lines. Reactive power is injected by the inverter in order to support the voltage. After disconnection, the voltage at the inverter goes back to its nominal value of 230.9 V reduced by the voltage drop introduced by the virtual impedance. The current before disconnection shows oscillations which are due to the calculation of RMS values with fixed window size. In the frequency signal, significant oscillations are observed before disconnection.

In Fig. 5, the RMS values of currents and voltages in exp1 are shown. For these, an asymmetry between the phases is observed. Both voltage and current of phase C are lower compared to phases A and B, which leads to oscillations in the 3-phase power measurement. Due to the P-f droop control,

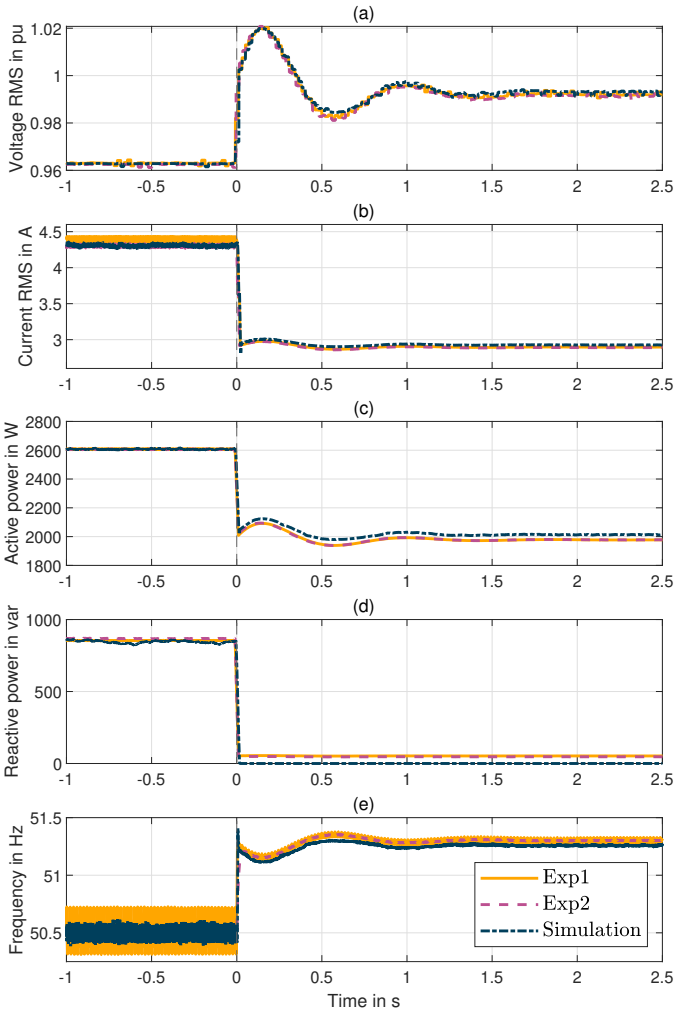

Fig. 4. Transition from grid connected to islanding mode. (a) inverter voltage, (b) inverter current, (c) inverter active power, (d) inverter reactive power, (e) inverter frequency.

these also lead to oscillations in the frequency observed in Fig. 4 (e). An explanation for the asymmetry in phase C of exp1 could not be identified, an error in the current measurement is suspected as the cause.

The steady state metrics for observed quantities are presented in Table II. The reactive power in the experiment after disconnection is 52.5 VAr for exp1 and 47 VAr for exp2, which in combination with the active power load of 2 kW is equivalent to a power factor of PF $= 0.9997$. The reactive power is explained by the resistance load used in the experiment having some parasitic inductance. The THD of voltages and currents is in good accordance between experiment and simulation, which is also reflected in the waveforms in Fig. 6.

In Fig. 6 and 7, the waveforms of voltages and currents during the disconnection are shown. After disconnection, voltage fluctuations can be observed in the experiment which are not present in the simulation results. Similarly, in the experiments the currents jump after disconnection in both magnitude and phase while they are continuous in the simulation.

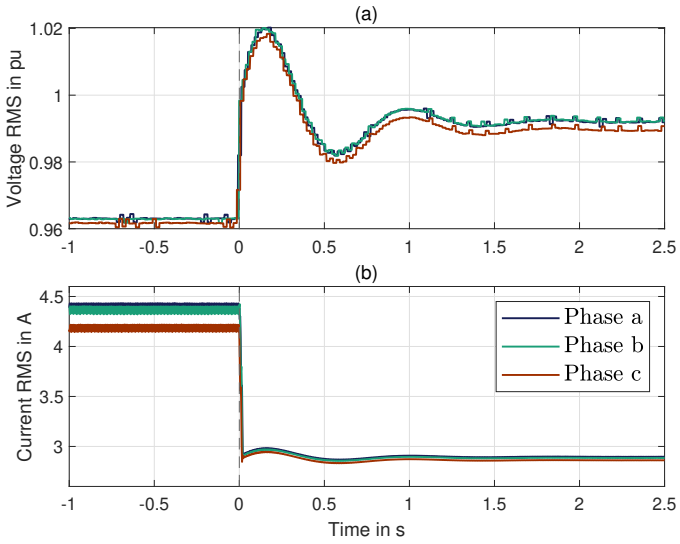

Fig. 5. Transition from grid connected to islanding mode. RMS phase values of (a) voltage and (b) currents of experiment 1.

TABLE II
STEADY STATE METRICS. MAXIMUM REFERS TO THE MAXIMUM OF THE THREE PHASES.

Quantity	operation mode	max. abs. rel. dev. to sim. [%]		max. THD [%]		
		Exp. 1	Exp. 2	Sim.	Exp. 1	Exp. 2
I_{rms}	grid conn.	3.39	0.62	5.59	7.64	6.30
	islanding	2.22	2.02	0.95	1.46	1.53
V_{rms}	grid conn.	0.12	0.19	0.33	0.78	0.58
	islanding	0.31	0.19	0.95	0.90	0.71
P	grid conn.	0.76	0.76			
	islanding	1.80	1.77			
Q	grid conn.	0.59	1.76			
	islanding	/	/			
f	grid conn.	0.05	0.05			
	islanding	0.09	0.09			

In the experiment, the load is reduced abruptly when the contactor is opened. The resulting load is lower compared to the connected state and mainly resistive. Thus, the currents amplitude jumps accordingly. A phase jump is also observed, as the inverter was providing reactive power in order to support the voltage level before disconnection. The observed voltage ripple after disconnection are likely to be explained by the current transients and their interaction with reactive filter elements and the control loop.

The different behavior of the simulation is caused by the utilized model of the three-phase circuit breaker. The simulated circuit breaker opens each phase separately at the next zero crossing of the respective phase current, while the physical contactor in the experiment disconnects all phases within less than a millisecond and irrespective of the momentary current values. Therefore, no jumps occur in the simulated currents and the voltage is not influenced.

V. IMPLEMENTATION CHALLENGES

A) Physical loads are usually not precisely symmetric which leads to oscillations in 3-phase power measurement. B) Due

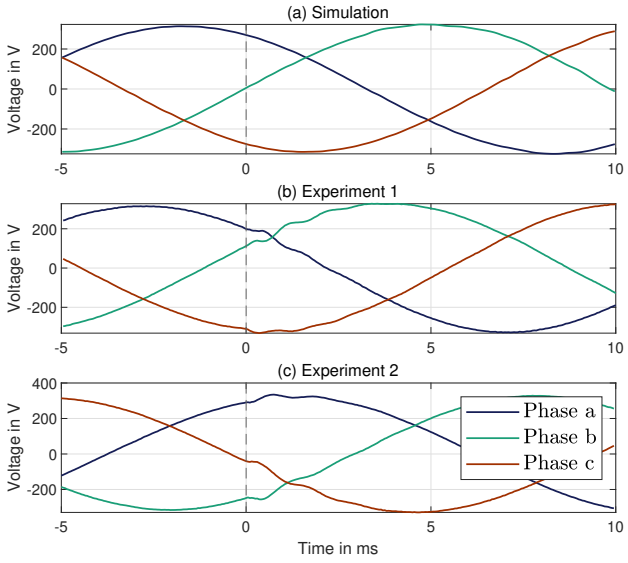

Fig. 6. Transition from grid connected to islanding mode. Voltage waveforms of (a) simulation, (b) experiment 1 and (c) experiment 2.

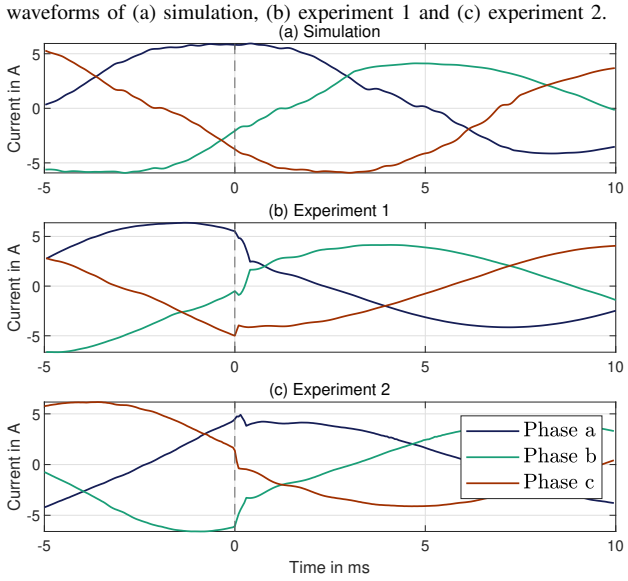

Fig. 7. Transition from grid connected to islanding mode. Current waveforms of (a) simulation, (b) experiment 1 and (c) experiment 2.

to asymmetries significant currents might flow in neutral conductors leading to slightly shifted voltages. C) Datasheet information on expected current sensor deviations might not always be accurate. Calibration in the operating point was found to be necessary. D) The hard switching of power electronics causes significant electro-magnetic interference (EMI). To reduce the EMI impact on the measurement transducers their position within the setup was found to be critical. E) Filters for EMI rejection are required but not all topologies are suitable. The deployed topology is shown in Fig. 3. Stray common mode currents were found to easily cause false tripping of the inverter protection.

VI. Conclusion

In this paper, the transition from grid-connected to islanding mode is analyzed for the exemplary case of a stand-alone grid forming inverter. Experimental results are compared to a simulation which utilizes the same control code. During the transition, the trend of considered quantities matches well for experiment and simulation. The deviation of steady state values is below 3.4 %. The experiments with different power semiconductors show slight differences in grid-connected operation, but the dynamic behavior is similar. Fast time scale transients after disconnection are not represented in the simulation as shown by the current waveform. Thus, for transient investigations on frequencies above the fundamental grid frequency, the performance and analysis of experiments is strongly recommended. Overall, the presented inverter provides a basis for further development and testing of control concepts.

References

[1] R. Rosso, X. Wang, M. Liserre, X. Lu, and S. Engelken, "Grid-Forming Converters: Control Approaches, Grid-Synchronization, and Future Trends—A Review," *IEEE Open Journal of Industry Applications*, vol. 2, pp. 93–109, 2021. [Online]. Available: https://ieeexplore.ieee.org/document/9408354/

[2] J. Wachter, L. Gröll, and V. Hagenmeyer, "Survey of Real-World Grid Incidents–Opportunities, Arising Challenges and Lessons Learned for the Future Converter Dominated Power System," *IEEE Open Journal of Power Electronics*, vol. 5, pp. 50–69, 2024. [Online]. Available: https://ieeexplore.ieee.org/document/10360292/

[3] S. D'silva, M. Shadmand, S. Bayhan, and H. Abu-Rub, "Towards Grid of Microgrids: Seamless Transition between Grid-Connected and Islanded Modes of Operation," *IEEE Open Journal of the Industrial Electronics Society*, vol. 1, pp. 66–81, 2020. [Online]. Available: https://ieeexplore.ieee.org/document/9072475/

[4] M. E. T. Souza and L. C. G. Freitas, "Grid-Connected and Seamless Transition Modes for Microgrids: An Overview of Control Methods, Operation Elements, and General Requirements," *IEEE Access*, vol. 10, pp. 97 802–97 834, 2022. [Online]. Available: https://ieeexplore.ieee.org/document/9888093/

[5] S. Fazal, M. E. Haque, M. T. Arif, and A. Gargoom, "Droop Control Techniques for Grid Forming Inverter," in *2022 IEEE PES 14th Asia-Pacific Power and Energy Engineering Conference (APPEEC)*. Melbourne, Australia: IEEE, Nov. 2022, pp. 1–6. [Online]. Available: https://ieeexplore.ieee.org/document/10072251/

[6] D. B. Rathnayake, M. Akrami, C. Phurailatpam, S. P. Me, S. Hadavi, G. Jayasinghe, S. Zabihi, and B. Bahrani, "Grid Forming Inverter Modeling, Control, and Applications," *IEEE Access*, vol. 9, pp. 114 781–114 807, 2021. [Online]. Available: https://ieeexplore.ieee.org/document/9513281/

[7] T. M. E. Abou Saltouh, A. E.-S. A. Nafeh, A. A. Abou El-Ela, F. H. Fahmy, and S. K. Nawar, "Control strategy for seamless transition between grid-connected and islanding modes in microgrid-based PV inverters," *Energy Systems*, vol. 14, no. 4, pp. 1135–1162, Nov. 2023. [Online]. Available: https://link.springer.com/10.1007/s12667-022-00528-1

[8] H. Mahmood and Jin Jiang, "A control strategy of a distributed generation unit for seamless transfer between grid connected and islanded modes," in *2014 IEEE 23rd International Symposium on Industrial Electronics (ISIE)*. Istanbul, Turkey: IEEE, Jun. 2014, pp. 2518–2523. [Online]. Available: http://ieeexplore.ieee.org/document/6865016/

[9] S.-H. Hu, C.-Y. Kuo, T.-L. Lee, and J. M. Guerrero, "Droop-controlled inverters with seamless transition between islanding and grid-connected operations," in *2011 IEEE Energy Conversion Congress and Exposition*. Phoenix, AZ, USA: IEEE, Sep. 2011, pp. 2196–2201. [Online]. Available: http://ieeexplore.ieee.org/document/6064059/

[10] M. Ganjian-Aboukheili, M. Shahabi, Q. Shafiee, and J. M. Guerrero, "Seamless Transition of Microgrids Operation From Grid-Connected to Islanded Mode," *IEEE Transactions on Smart Grid*, vol. 11, no. 3, pp. 2106–2114, May 2020. [Online]. Available: https://ieeexplore.ieee.org/document/8869850/

[11] D. S. Ochs, B. Mirafzal, and P. Sotoodeh, "A Method of Seamless Transitions Between Grid-Tied and Stand-Alone Modes of Operation for Utility-Interactive Three-Phase Inverters," *IEEE Transactions on Industry Applications*, vol. 50, no. 3, pp. 1934–1941, May 2014. [Online]. Available: http://ieeexplore.ieee.org/document/6605553/

[12] C. Bischoff, D. Schulz, S. Mersche, L. Stefanski, and M. Hiller, "Design and Implementation of Grid-Forming Control Strategies for Parallel Converters in an Islanded Microgrid Setup," in *2023 25th European Conference on Power Electronics and Applications (EPE'23 ECCE Europe)*. Aalborg, Denmark: IEEE, Sep. 2023, pp. 1–9. [Online]. Available: https://ieeexplore.ieee.org/document/10264548/

[13] A. Cardenas and K. Agbossou, "Experimental Evaluation of Voltage Positive Feedback Based Anti-Islanding Algorithm: Multi-Inverter Case," *IEEE Transactions on Energy Conversion*, vol. 27, no. 2, pp. 498–506, Jun. 2012. [Online]. Available: http://ieeexplore.ieee.org/document/6170550/

[14] L. K. Gan, J. K. Shek, and M. A. Mueller, "Modelling and experimentation of grid-forming inverters for standalone hybrid wind-battery systems," in *2015 International Conference on Renewable Energy Research and Applications (ICRERA)*. Palermo, Italy: IEEE, Nov. 2015, pp. 449–454. [Online]. Available: http://ieeexplore.ieee.org/document/7418453/

[15] R. Mittal, Z. Miao, and L. Fan, "Grid Forming Inverter: Laboratory-Scale Hardware Test Bed Setup and Weak Grid Operation," in *2021 North American Power Symposium (NAPS)*. College Station, TX, USA: IEEE, Nov. 2021, pp. 1–6. [Online]. Available: https://ieeexplore.ieee.org/document/9654589/

[16] M. Amin and Q.-C. Zhong, "Resynchronization of Distributed Generation Based on the Universal Droop Controller for Seamless Transfer Between Operation Modes," *IEEE Transactions on Industrial Electronics*, vol. 67, no. 9, pp. 7574–7582, Sep. 2020. [Online]. Available: https://ieeexplore.ieee.org/document/8848788/

[17] R. Ortega, O. Carranza, J. J. Rodriguez, V. H. Garcia, J. C. Sosa, and J. M. Alvarado, "Development and Application of a Reconfigurable Photovoltaic Inverter for Operation Within a Microgrid," *IEEE Access*, vol. 7, pp. 98 755–98 770, 2019. [Online]. Available: https://ieeexplore.ieee.org/document/8766830/

[18] A. Winkens, I. Contu, P. Linnartz, and A. Ulbig, "Experimental Validation of the Parallel Operation of Grid-Forming Converters and Synchronous Generators in Temporary Islanded Microgrids," in *2022 International Conference on Smart Energy Systems and Technologies (SEST)*. Eindhoven, Netherlands: IEEE, Sep. 2022, pp. 1–6. [Online]. Available: https://ieeexplore.ieee.org/document/9898480/

[19] "EN 50160:2022 Voltage characteristics of electricity supplied by public electricity networks."

[20] J. Rocabert, A. Luna, F. Blaabjerg, and P. Rodríguez, "Control of Power Converters in AC Microgrids," *IEEE Transactions on Power Electronics*, vol. 27, no. 11, pp. 4734–4749, Nov. 2012. [Online]. Available: http://ieeexplore.ieee.org/document/6200347/

[21] F. Wiegel, J. Wachter, M. Kyesswa, R. Mikut, S. Waczowicz, and V. Hagenmeyer, "Smart Energy System Control Laboratory – a fully-automated and user-oriented research infrastructure for controlling and operating smart energy systems," *at - Automatisierungstechnik*, vol. 70, no. 12, pp. 1116–1133, Dec. 2022.